A new method for determining the total electron content in Mars' ionosphere based on Mars Express MARSIS data

Philip Conroy[a], Gary Quinsac[a], Nicolas Floury[a], Olivier Witasse[a,*], Marco Cartacci[b], Roberto Orosei[c], Wlodek Kofman[d,e], Beatriz Sanchez-Cano[f]

[a] *European Space Agency, ESTEC, Keplerlaan 1, 2201 AZ Noordwijk, The Netherlands*
[b] *Istituto Nazionale di Astrofisica (INAF), Istituto di Astrofisica e Planetologia Spaziali (IAPS), Rome, Italy*
[c] *Istituto di Radioastronomia (IRA), Istituto Nazionale di Astrofisica (INAF), Bologna, Italy*
[d] *Univ. Grenoble Alpes, CNRS, CNES, IPAG, 38000 Grenoble, France*
[e] *Space Research Centre, PAN, Warsaw, Poland*
[f] *Radio and Space Plasma Physics Group, Department of Physics and Astronomy, University of Leicester, University Road, Leicester, LE1 7RH, UK*

Abstract

We present a new method for determining the total electron content (TEC) in the Martian ionosphere based on the time delay of received radar pulses of the Mars Advanced Radar for Subsurface and Ionospheric Sounding (MARSIS) on board the Mars Express spacecraft. Previous studies of the same dataset have produced differing results for the day-side ionosphere, so it is useful to have an alternative way to compute the TEC in this region. This method iterates a model ionosphere in order to simultaneously match the ionospheric delays of the signals received by the radar's two channels by finding the model which minimizes the root mean square error (RMSE) between

*Corresponding author
Email address: owitasse@cosmos.esa.int (Olivier Witasse)

the measured and simulated delays. Topographical information is obtained from data from the Mars Orbiter Laser Altimeter (MOLA) instrument. The model parameters are held constant for a given orbit, and a very good agreement between the simulated and measured delays is obtained. The TEC can then be inverted from the ionospheric model. Matching the delays of both channels simultaneously applies an additional constraint to the model which has not been made in previous studies. The model is additionally validated by matching the simulated pulses with the raw range-compressed measurements for one orbit. Finally, typical model parameters are compared to those obtained by previous studies, which are also simulated. The method is applied to orbits during moderate solar activity, and results show very good agreement with previous studies.

Keywords:

Mars, MARSIS, MOLA, Ionosphere, Total electron content

---

1. Introduction

The ionosphere of Mars has been studied over more than 40 years, and since the start of the Mars Global Surveyor and Mars Express missions, and more recently with the Mars Atmosphere and Volatile Evolution (MAVEN) mission, a large and continuous dataset of plasma measurements has been collected. In particular, the Mars Advanced Radar for Subsurface and Ionospheric Sounding (MARSIS) instrument on board Mars Express routinely provides the Total Electron Content (TEC). This is a very useful parameter to characterise the ionosphere and to study its variability as a function of solar illumination, Martian season, and solar and space weather activity.

The computation of the TEC from the processing of radar data is not a straightforward process and differences have been found between different works, especially on the day-side [1]. In [2] and [3], a numerical expansion of the refractive index is made to model the phase distortion of the signal. The expansion terms are estimated by an optimization method which tries to maximize the signal-to-noise ratio (SNR) of the received signal at one point in the orbit. This allows for a compensation of the distortion and an estimation of the TEC. Another method which is documented in [4] and [5] is based on the output from an algorithm known as the contrast method (CM), which is used during processing of the raw signal to compensate for higher-order distortion which causes blurring in the obtained radargram. A radargram is a bi-dimensional colour-coded diagram made of a sequence of echoes in which the horizontal axis is the distance along the ground track of the spacecraft, the vertical axis represents the two-way travel time of the echo, and brightness is a function of the received echo power. This method assumes that the radar signal is narrow-banded by making a Taylor expansion around the central frequency to approximate the differential phase change across the band of the received signal. The expansion terms are algebraically related to the TEC, which can then be solved for.

In this study, we show a new method in deriving the TEC, still based on the same MARSIS data set. Instead of deriving the TEC by analysing the high order distortion, we use the time delay recorded on both radar frequencies, for the entire portion of the orbit over the planet's day side. We have used the radar data that has recently become available in the European Space Agency's (ESA) Planetary Science Archive (PSA). This gives us a new

way to obtain the TEC by analysing a different aspect of the ionospheric distortion. Grima et al. [6] describe the effects of the ionosphere's dispersive phase shift in the time domain in the context of future radar sounders to be sent to Europa, and show how the TEC may be estimated with differential delay times by using the first expansion term of the refractive index described in [2] and [3]. Scanlan et al. [7] use the method proposed in [6] to estimate the TEC on Mars by combining MARSIS and SHARAD data.

Section 2 briefly describes the ionospheric effects encountered by a radar signal in the Martian ionosphere and Section 3 describes the MARSIS instrument itself. Section 4 documents a simulation tool which is developed to model the distortion of a MARSIS radar pulse, and Section 5 describes the TEC inversion method which is developed. Results are presented and discussed Section in 6 and conclusions are drawn in Section 7.

2. Ionospheric Effects on the Radar Signal

The Martian ionosphere is a dispersive medium, which in the absence of a magnetic field has a refractive index n given by

$$n(\omega, z) = \sqrt{1 - \frac{\omega_p^2(z)}{\omega^2 - i\omega\nu(z)}} \tag{1}$$

where z is the vertical coordinate, $\omega_p(z)$ is the angular plasma frequency, ω is the angular frequency of the electromagnetic wave propagating through it, and $\nu(z)$ is the electron-neutral collision frequency. Neglecting absorption (by setting the imaginary component to zero), the wave number k of the pulse is

$$k(\omega, z) = \frac{1}{c}\sqrt{\omega^2 - \omega_p^2(z)} \tag{2}$$

This simplification is valid because $\nu(z)$ generally ranges from 10-60 kHz and is small compared to the frequencies of the MARSIS bands [8]. During solar storms this no longer applies and absorption has a significant effect on the signal [9]. Equation (2) can be expanded numerically for a small ω_p/ω. Keeping the first three terms gives the result

$$k(\omega, z) \approx \frac{\omega}{c} - \frac{\omega_p^2}{2\omega c} - \frac{\omega_p^4}{8\omega^3 c} \tag{3}$$

A detailed treatment of these equations is given in [10]. The time delay of a radar pulse is given by

$$\Delta t_{iono}(\omega) = \frac{1}{c\omega^2} \int_0^\infty \omega_p^2(z) dz + \frac{3}{4c\omega^4} \int_0^\infty \omega_p^4(z) dz \tag{4}$$

Note that a factor of 2 has been multiplied through the right-hand side to reflect that there are two ionospheric crossings, which corresponds to a radar pulse travelling down from the satellite, reflecting off the surface and travelling back up towards the satellite.

3. MARSIS Instrument

A detailed description of the MARSIS instrument can be found in [11]. MARSIS can operate in multiple modes. In this work, the data collected during the subsurface sounding 3 (SS3) mode is used. The radar transmits two linear frequency modulated waveforms (chirps) with 1 MHz bandwidth in quick succession. The two chirps are each centred on a different frequency, corresponding to one of the radar's four operating bands: 1.8 MHz (band 1), 3 MHz (band 2), 4 MHz (band 3), or 5 MHz (band 4). Thus it can be said that in the SS3 mode, MARSIS simultaneously collects data on two different bands.

The onboard processing is described in greater detail in [5]. The received signal is first azimuth and then ranged compressed. Azimuth compression of pulse echoes consists in artificially adding a delay, corresponding to a phase shift of the complex signal, to the samples of each pulse, and then in summing the samples so as to allow the constructive sum of the signal component whose delay (phase shift) from one pulse to the next corresponds to a desired direction (usually nadir or close to nadir). Range processing consists of computing the mathematical correlation between the transmitted pulse and received echoes. Initially it was intended for the range compression to be carried out onboard the satellite by the CM, an algorithm developed to remove higher-order distortion from the signal. During the commissioning phase it was found that the system implemented onboard was malfunctional, and so it was subsequently disabled. This means that the higher-order distortion which the CM was meant to remove, including broadening of the signal in time, is still present. This is step therefore now completed on the ground. The subsequent processing step tracks the signal position inside the receiving window to provide timing information about the received signal.

4. Ionospheric Delay Simulation

4.1. Motivation

The discrepancies between the results of different ionosphere distortion correction methods motivated the development of a simulator which models the effect of the Martian ionosphere on a radar pulse sent by MARSIS. This allows us to find the expected time delay of a radar pulse from a theoretical basis and provides a neutral starting point with which to assess the collected

MARSIS data. A similar tool was developed in [12] to model Martian ionospheric effects.

4.2. Radar Pulse Synthesis and Propagation

An ideal linear chirp with 1 MHz bandwidth and 250 μs pulse length is synthesised on one of the four MARSIS bands, corresponding to the system specifications. This transmitted signal propagates from the spacecraft down to the surface, is reflected, and propagates back toward the spacecraft where it is received. Reflection on the ground is approximated to be specular since no a priori information about the subsurface is available, and no terrain or clutter is simulated. The ionospheric simulation calculates the extra time delay caused by two crossings of the ionosphere. Since we are only interested in the delay, effects such as turbulence and Faraday rotation are not considered.

The ionosphere is divided into layers of height $\Delta h = 500$ m each, in which the electron density is constant. This number of layers ensures that discontinuities between each layer are very small, such that spurious reflections between the layers are not significant. This corresponds to dividing the simulation space into 1000 layers. The refractive index is found using the unmagnetized dispersion relation given in equation (1). At the interface between each layer, the transmission coefficient is determined using

$$T_{m+1} = \frac{2n_m}{n_{m+1} + n_m} \tag{5}$$

where n_m is the refractive index of the mth layer. The wave S is propagated between layers by

$$S_{m+1} = T_{m+1} \cdot S_m e^{-i\Delta k_{m+1}\Delta h} \tag{6}$$

where Δk is the relative change in wave number with respect to free space, given by

$$\Delta k_m = \frac{\omega}{c} \cdot (n_m - 1) \tag{7}$$

Following reflection by the ground, the ionospheric layers are inverted and the signal is propagated through again. Reflection from the ground. The refractive index for a given ionospheric layer is calculated using equation (1). The electron density at a given point in the ionosphere is modelled using a Chapman layer. The model is created using the methodology described in Section 5.

4.3. Determining the Time Delay

The pulse is compressed by correlating the spectrum of the received pulse, $S_r(f)$ with a copy of the spectrum of the original, undistorted pulse, $S_t(f)$, where f is the frequency. The time delay of the signal, Δt_{iono}, is taken as the delay which corresponds to the centre of mass (COM) of the pulse [10]. The correlation magnitude is given by

$$C(\tau) = \chi(\tau)\bar{\chi}(\tau) \tag{8}$$

where the bar indicates the complex conjugate, τ is the time delay coordinate used in the correlation, and $\chi(\tau)$ is

$$\chi(\tau) = \int S_t(f)\bar{S}_r(f)e^{-2\pi f\tau}df \tag{9}$$

The delay of the signal, Δt_{iono}, is then given by

$$\Delta t_{iono} = \tau_{COM} = \frac{\int \tau \cdot C(\tau)d\tau}{\int C(\tau)d\tau} \tag{10}$$

Additionally, the leading edge of the pulse can be estimated using the "offset centre of gravity" (OCOG) method [13]. This method is used by MARSIS during processing of the low-level data [5]. The half-width of the pulse, $\tau_{W/2}$ is estimated and subtracted from the COM position:

$$\Delta t_{OCOG} = \tau_{COM} - \tau_{W/2} \tag{11}$$

where $\tau_{W/2}$ is given by

$$\tau_{W/2} = \frac{\left(\int C(\tau)d\tau\right)^2}{2 \cdot \int C^2(\tau)d\tau} \tag{12}$$

An example of a compressed pulse is shown in Figure 1. In this case the time delay is found to be approximately 62 μs.

5. Total Electron Content Retrieval

5.1. Matching the Ionospheric Time Delay

Inverting the TEC from an ionospheric model is challenging because many assumptions have to be made, and there are not many constraints which can be placed on the model [2], [5], [14]. Therefore the objective of the simulation used in this work is to find an ionospheric model which can satisfy equation (4) for both channels simultaneously. The radar sends pulses centred on 4 and 3 MHz, or 5 and 4 MHz. Due to the dispersive nature of the ionosphere, the terms in equation (4) are weighted by frequency. Therefore, finding a model which matches the delays recorded by both channels constitutes finding a solution for $\omega_p(z)$ in the system of equations

$$\Delta t_1 = \frac{1}{c\omega_1^2}\int_0^\infty \omega_p^2(z)dz + \frac{3}{4c\omega_1^4}\int_0^\infty \omega_p^4(z)dz$$
$$\Delta t_2 = \frac{1}{c\omega_2^2}\int_0^\infty \omega_p^2(z)dz + \frac{3}{4c\omega_2^4}\int_0^\infty \omega_p^4(z)dz \quad (13)$$

The ionospheric delay output by the simulator is compared to the delay measured by the radar on both channels. The data used for this comparison comes from the reduced data record (RDR) dataset available in the ESA PSA. The full description of this dataset is available in [15]. This data has already been compressed in azimuth and range, and has been focused by the CM to remove ionospheric distortion, apart from the time delay. The time delay present in the signal is the sum of the free-space and ionospheric delays. The free-space delay is derived from altimetry data recorded by the MOLA instrument, and subtracted from the total delay, leaving only the ionospheric component. The total delay is extracted from the RDR radargram by finding the first sample of each frame with an SNR $>$ 20 dB. This technique is used to minimize the effect of subsurface reflections on the time delay measured with respect to the surface [5]. The free-space delay is given by

$$\Delta t_{fs} = \frac{2 \cdot (25\text{km} - z_{MOLA})}{c} \quad (14)$$

where z_{MOLA} is the height of the surface above the Martian ellipsoid as defined in [16]. The 25 km in equation (14) refers to the fact that the RDR dataset has already been aligned to a reference height of 25 km above the planet's surface [15].

The ionospheric delay derived from the RDR dataset is compared on a frame-by-frame basis with the simulated ionospheric delay. A single-layer

Chapman model is iteratively tuned such that the RMSE between the simulated and measured delay is minimized. The Chapman layer is defined in [17] by

$$N_e(z) = N_{e_0} \cdot \exp\left(\frac{1}{2}\big[1 - h - Ch\left(z, \chi\right) \cdot \exp\left(-z\right)\big]\right) \tag{15}$$

where $N_e(z)$ is the electron density in m^{-3} at a given height z. N_{e_0} is the maximum electron density with corresponding height z_0, χ is the solar zenith angle, and $h(z)$ is given by

$$h = \frac{z - z_0}{H} \tag{16}$$

where H is the scale height. Finally, $Ch(z, \chi)$ is the Chapman grazing incidence function, given in [17] by

$$Ch(z, \chi) = d \sin\chi \int_0^{\chi} \exp\left(d - d\frac{\sin\chi}{\sin\alpha}\right) \csc^2\alpha \mathrm{d}\alpha \tag{17}$$

where

$$d = \frac{R + z}{H} \tag{18}$$

and R is the radius of the planet, equal to 3390 km.

The maximum density height is fixed to a typical value of 130 km. The location of the maximum density point is relatively stable and well-established [2] [18]. This assumption is required in order to constrain the degrees of freedom in the modelling problem. Since a Chapman profile is a function of 3 parameters, there exist multiple Chapman profiles which can solve the system of equations in (13). The model is then tuned by changing either the scale height or the peak electron density of the Chapman layer. However in practice, both parameters have similar effects, but changing the scale height causes the TEC to "rise" faster as SZA decreases, as noted in [3]. An

optimum combination of parameters is found by sweeping through several starting values of H and allowing the algorithm to optimize for N_{e0}.

The combination of scale height and peak electron density which minimizes the RMSE is found for each orbit which is processed. The nominal values for these two parameters at the sub-solar point (SZA = 0 degrees) are held constant for that orbit, however, their values scale throughout the orbit with SZA as per equation (15). While local variations (for instance those caused by the crustal magnetic field) are lost, a very good agreement with the mean delay can be found. A similar modelling approach is used in [2] to derive parameters for a best-fit Chapman profile.

For SZAs greater than 95 degrees, the simulator does not capture the effects of the night-time ionosphere, because the simulated delay tends to zero as a consequence of the Chapman grazing function, but other effects not taken into account by the Chapman model, such as plasma transport, become significant near the terminator [19]. For SZAs below 60 degrees, distortion becomes very significant and it is difficult to recover a signal. Therefore, the region of SZA used to calculate the RMSE is constrained between 60 and 90 degrees.

5.2. Reproducing the Distorted Pulses

The optimum ionospheric profile obtained through the RMSE minimization routine can be further validated by comparing the distorted pulses it simulates to the raw range-compressed data which has not been focused by the ionosphere. Multiple reflections from the subsurface can make comparison difficult, but in these cases rising edge of the pulse shows a agreement with the raw data, as can be seen in Figure 2a. In cases with a strong sur-

face reflection, the general shape of the raw pulse matches sufficiently well the simulation result, as is the case in Figure 2b. This step is performed as an extra check to validate the simulated pulses, but is not used to invert the TEC.

6. Results and Discussion

6.1. Ionospheric Model

The Martian ionosphere is modeled in the simulator using a Chapman layer whose electron density and scale height are iteratively tuned to match the observed delay of the radar pulse. The profile obtained through RMSE minimization for orbit 4646 and a SZA of 70 degrees is shown in Figure 3. The model parameters are given in Table 1. The starting iteration used for the model parameters are taken from the best-fit Chapman parameters described in [14]. The maximum density height is also taken from [14] and held constant.

Table 1: Best-fit ionospheric model parameters at SZA = 0 degrees (Orbit 4646)

Parameter	Value
Neutral scale height	15.2 km
Maximum electron density	$1.29 \cdot 10^{11}$ m^{-3}
Maximum density height	130 km
Vertical step size	500 m
Simulation range	0-500 km
F10.7 (measured at Earth)	67.3 sfu
Mars-Sun distance	1.42 AU

6.2. Comparison of Measured and Simulated Delays

The measured and simulated ionospheric delays of orbit 4646 for both channels are plotted against SZA in Figure 4. The agreement between measurement and simulation is very close, and the combined RMSE for both channels is 4.184 μs.

6.3. Total Electron Content: Orbits 4640-4649

The TECs obtained by the algorithm for orbits 4640-4649 are shown in Figure 5, and the mean TEC obtained for orbits 4640-4649 is compared to the results of other studies in Figure 6. A moving average filter is used to find the mean results of Cartacci et al. [5] and Mouginot et al. [3] in order to allow for better readability in the figure. The NeMars model [20] using parameters derived in [18] is plotted for a portion of the orbit, because the model is only valid for the dayside. A mismatch can be found between NeMars and our TEC determination. This is not surprising, first because such disagreement was already identified in [1]. The NeMars TEC are closer to the values from Cartacci et al. Secondly, and more generally, an agreement between data and model is usually difficult to achieve, given the variability of the Mars' atmosphere (e.g. see [21] section 2.2.2.). In any case, such mismatch between the different data sets speak for the need of a new critical comparison of the various TEC data processing pipelines, which should be discussed in view of this article. A good agreement is found between our inversion algorithm and Mouginot et al., and we also find a close agreement with the results of [2].

Data from the active ionospheric sounding (AIS) mode [14] is not available while MARSIS is operating in the SS3 mode, but the best-fit Chapman profile obtained from the AIS data [14] is plotted for comparison for the entire range

of SZA studied. The AIS mode of MARSIS allows the topside of the main ionospheric layer to be probed, but it cannot collect any data on the bottom side of the main layer, nor any secondary layers which may exist beneath the main layer. Therefore, the AIS-fitted model should be considered as lower bound on the TEC. Also note that the model is derived from measurements taken during periods of solar activity with F10.7 values of 72-119 sfu, while orbits 4640-4649 took place during F10.7 levels of 67.5 sfu, and so a somewhat weaker ionosphere can be expected than that given by the AIS-fitted model.

6.4. Total Electron Content: Orbit 8762

The algorithm is run for orbit 8762 in order to provide a point of comparison during solar activity levels corresponding to the AIS-fitted model in [14]. The orbit occurred during a period of moderate solar activity as defined in [18]. This orbit is selected because the F10.7 measured during this time is 84 sfu, which corresponds to the mean value of F10.7 for the measurements considered in [14]. The best-fit model parameters obtained for this orbit are shown in Figure Table 2. The TEC is plotted against SZA in Figure 7, where it can be seen that during conditions of moderate solar activity, the TEC inverted from the algorithm is greater than that obtained by the AIS-fitted model, which only considers the main ionospheric layer. Due to the presence of a secondary layer during moderate solar activity [20], we can expect the TEC of the entire ionosphere to be approximately 10% greater than the Gurnett et al. model.

The algorithm does not consider local variations in the TEC, and neither does the Gurnett et al. best-fit model. This can be seen in Figure 7, when there are local "dips" in TEC, at 80 and 85 degrees SZA in the results of

[5] and [3], this is not reflected in the results of our inversion algorithm. However, apart from these local deviations, a good agreement is found with [3].

Table 2: Best-fit ionospheric model parameters at SZA = 0 degrees (Orbit 8762)

Parameter	Value
Neutral scale height	14 km
Maximum electron density	$1.63 \cdot 10^{11}$ m^{-3}
Maximum density height	130 km
Vertical step size	500 m
Simulation range	0-500 km
F10.7 (measured at Earth)	84 sfu
Mars-Sun distance	1.47 AU

6.5. Summary

The TEC inverted from the best-fit model tends to agree with that found by [3] in cases of low and moderate solar activity. During low solar activity, the TEC obtained by our inversion algorithm also matches closely with TEC given by the AIS-fitted model. This can be explained by the fact that we do not expect a secondary ionospheric layer to be present during solar minimum. During moderate solar activity, our algorithm provides a TEC which again matches closely with [3], and is approximately 10% greater than the TEC given by the AIS-fitted model at 70 degrees SZA. In this case, we expect a secondary ionospheric layer to be present and to contribute to approximately 10% of the TEC, and so we can conclude that here we also have results which

are consistent with what the AIS-fitted model provides.

6.6. Sources of Error

The ionospheric model derived in this work best fits the ionospheric delay measurement data obtained from the level 3 data available in the ESA PSA. However, the following potential sources of error may affect this result (and those of other studies):

- The best-fit Chapman profile is an idealization and the true ionosphere may have a different morphology. However, the simultaneous minimization on both channels of the RMSE between the simulated and measured delay times ensures that the terms of the system of equations in (13) are weighted correctly.

- The algorithm fits a single Chapman profile to the range of SZA under consideration. Therefore, local variations in the TEC are lost, and some residual error remains after an optimal ionospheric profile has been found, and is visible in Figure 4. This residual RMS error is approximately ± 0.03 TECu.

- The algorithm operates on level 3 data from the PSA. This data has already been processed: azimuth- and range-compressed, aligned to a reference altitude, and ionospheric focusing applied. Any errors introduced by the upstream processing of this data will have an effect on the final result.

7. Conclusion

A novel method for TEC estimation based on analysing the ionospheric time delay in the MARSIS radar signals is developed. The algorithm is computationally inexpensive compared to other methods, and can be used with publicly available data in the ESA Planetary Science Archive. The method uses an ionospheric model which is iterated in order to match the real delay experienced by the signals received on both channels of the radar. The dual-frequency approach is a novel one, and provides an additional constraint in determining the correct model. The iterated model is further verified by comparing the distorted pulse shapes it simulates with raw range-compressed pulses taken from the radar measurements, and the simulated profile can reproduce the raw pulses in cases of strong surface reflection. In cases of moderate solar activity, the TEC obtained by this study is consistent with the best-fit ionospheric model obtained from AIS data, and also agrees well with previous studies using SS3 data.

Acknowledgements

The authors would like to thank the ESA Young Graduate Trainee program, the ESA Internship program, and the staff and faculty of ESTEC for supporting this study. We would also like to thank both the MARSIS and ESA teams who worked to archive the great amount of data in the PSA. The PSA can be accessed via https://archives.esac.esa.int/psa. Finally, thank you to J. Mouginot for providing a sample of raw range-compressed data to assist this study.

References

[1] B. Sánchez-Cano, D. Morgan, O. Witasse, S. Radicella, M. Herraiz, R. Orosei, M. Cartacci, A. Cicchetti, R. Noschese, W. Kofman, C. Grima, J. Mouginot, D. Gurnett, M. Lester, P.-L. Blelly, H. Opgenoorth, and G. Quinsac, "Total electron content in the martian atmosphere: A critical assessment of the mars express marsis data sets," *Journal of Geophysical Research: Space Physics*, 2015.

[2] A. Safaeinili, W. Kofman, J. Mouginot, Y. Gim, A. Herique, A. Ivanov, J. Plaut, and G. Picardi, "Estimation of the total electron content of the martian ionosphere using radar sounder surface echoes," *Geophysical Research Letters*, vol. 34, no. 23, 2007.

[3] J. Mouginot, W. Kofman, A. Safaeinili, and A. Herique, "Correction of the ionospheric distortion on the marsis surface sounding echoes," *Planetary and Space Science*, vol. 56, no. 7, pp. 917 – 926, 2008.

[4] M. Cartacci, E. Amata, A. Cicchetti, R. Noschese, S. Giuppi, B. Langlais, A. Frigeri, R. Orosei, and G. Picardi, "Mars ionosphere total electron content analysis from marsis subsurface data," *Icarus*, vol. 223, no. 1, pp. 423 – 437, 2013.

[5] M. Cartacci, B. Sánchez-Cano, R. Orosei, R. Noschese, A. Cicchetti, O. Witasse, F. Cantini, and A. Rossi, "Improved estimation of mars ionosphere total electron content," *Icarus*, vol. 299, pp. 396 – 410, 2017.

[6] C. Grima, D. D. Blankenship, and D. M. Schroeder, "Radar signal prop-

agation through the ionosphere of europa," *Planetary and Space Science*, vol. 117, pp. 421 – 428, 2015.

[7] K. M. Scanlan, C. Grima, G. Steinbrügge, S. D. Kempf, D. A. Young, and D. D. Blankenship, "Geometric determination of ionospheric total electron content from dual frequency radar sounding measurements," *Planetary and Space Science*, p. 104696, 2019.

[8] K. Davies, *Ionospheric Radio*. IEE, 3 ed., 1989.

[9] B. Sánchez-Cano, P.-L. Blelly, M. Lester, O. Witasse, M. Cartacci, R. Orosei, H. Opgenoorth, R. Lillis, F. Leblanc, S. E. Milan, P. Conroy, N. Floury, J. M. Plane, A. Cicchetti, R. Noschese, and A. J. Kopf, "Origin of the extended mars radar blackout of september 2017," *Journal of Geophysical Research: Space Physics*, vol. 0, no. ja, 2019.

[10] N. A. Armand, V. M. Smirnov, and T. Hagfors, "Distortion of radar pulses by the martian ionosphere," *Radio Science*, vol. 38, no. 5, 2003.

[11] R. Jordan, G. Picardi, J. Plaut, K. Wheeler, D. Kirchner, A. Safaeinili, W. Johnson, R. Seu, D. Calabrese, E. Zampolini, A. Cicchetti, R. Huff, D. Gurnett, A. Ivanov, W. Kofman, R. Orosei, T. Thompson, P. Edenhofer, and O. Bombaci, "The mars express marsis sounder instrument," *Planetary and Space Science*, vol. 57, no. 14, pp. 1975 – 1986, 2009.

[12] O. N. Rzhiga, "Distortions of the low frequency signal by martian ionosphere at vertical propagation," *IEEE Transactions on Antennas and Propagation*, vol. 53, pp. 4083–4088, Dec 2005.

[13] D. Wingham, C. Rapley, and H. Griffiths, "New techniques in satellite altimeter tracking systems," in *Proceedings of IGARSS*, vol. 86, pp. 1339–1344, 1986.

[14] D. Gurnett, R. Huff, D. Morgan, A. Persoon, T. Averkamp, D. Kirchner, F. Duru, F. Akalin, A. Kopf, E. Nielsen, A. Safaeinili, J. Plaut, and G. Picardi, "An overview of radar soundings of the martian ionosphere from the mars express spacecraft," *Advances in Space Research*, vol. 41, no. 9, pp. 1335 – 1346, 2008.

[15] R. Orosei, R. L. Huff, A. B. Ivanov, and R. Noschese, *Mars Express - MARSIS To Planetary Science Archive Interface Control Document*, 4.1 ed., Dec. 2017.

[16] T. C. Duxbury, R. L. Kirk, B. A. Archinal, and G. A. Neumann, "Working group recommendations on mars cartographic constants and coordinate systems," in *Symposiumon Geospatial Theory, Processing and Applications*, (Ottawa, Canada), 2002.

[17] S. Chapman, "The absorption and dissociative or ionizing effect of monochromatic radiation in an atmosphere on a rotating earth," *Proceedings of the Physical Society*, vol. 43, pp. 26–45, jan 1931.

[18] B. Sánchez-Cano, M. Lester, O. Witasse, S. E. Milan, B. E. S. Hall, M. Cartacci, K. Peter, D. D. Morgan, P.-L. Blelly, S. Radicella, A. Cicchetti, R. Noschese, R. Orosei, and M. Pätzold, "Solar cycle variations in the ionosphere of mars as seen by multiple mars express data

410 sets," *Journal of Geophysical Research: Space Physics*, vol. 121, no. 3,
411 pp. 2547–2568, 2016.

412 [19] J. L. Fox and K. E. Yeager, "Morphology of the near-terminator martian
413 ionosphere: A comparison of models and data," *Journal of Geophysical*
414 *Research: Space Physics*, vol. 111, no. A10, 2006.

415 [20] B. Sánchez-Cano, S. Radicella, M. Herraiz, O. Witasse, and
416 G. Rodríguez-Caderot, "Nemars: An empirical model of the martian
417 dayside ionosphere based on mars express marsis data," *Icarus*, vol. 225,
418 no. 1, pp. 236 – 247, 2013.

419 [21] N. Mangold, D. Baratoux, O. Witasse, T. Encrenaz, and C. Sotin,
420 "Mars: a small terrestrial planet," *The Astronomy and Astrophysics*
421 *Review*, vol. 24, p. 15, Nov 2016.

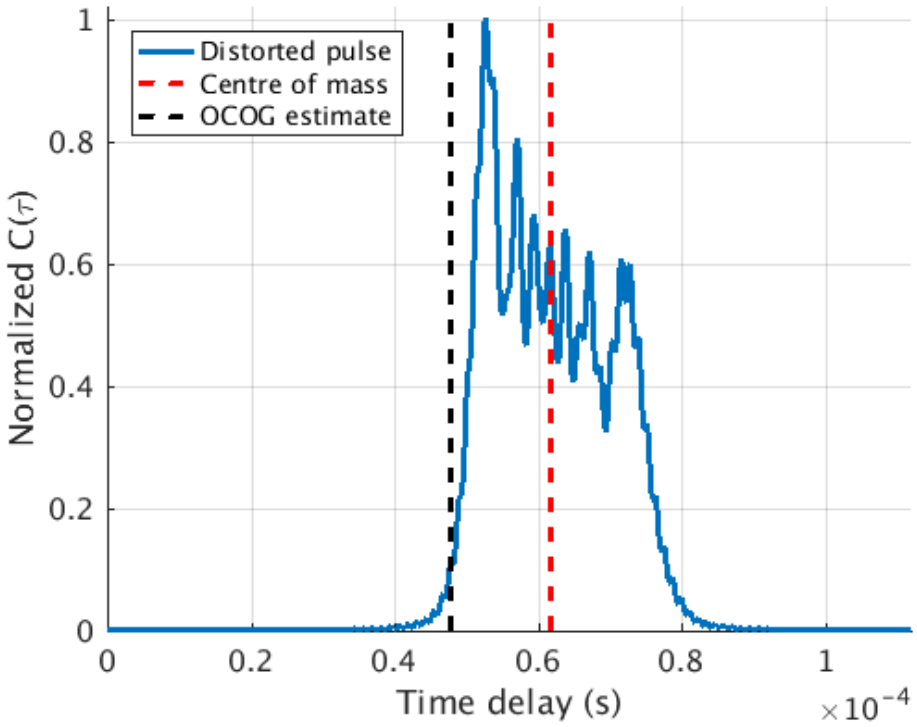

Figure 1: Determining the time delay of the radar pulse. The y-axis is the magnitude of the distorted, compressed pulse found by correlation of the transmitted and received signals. The axis is normalized such that the maximum correlation with an undistorted pulse equals unity. Red dashed line: COM delay. Black dotted line: OCOG delay.

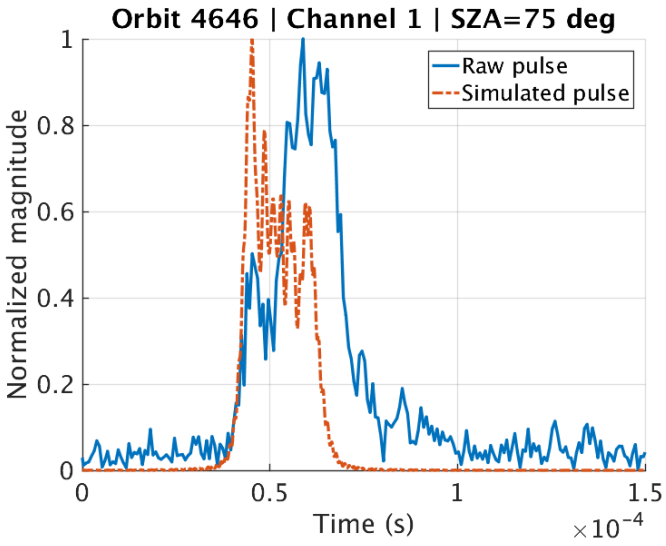

(a) Channel 1.

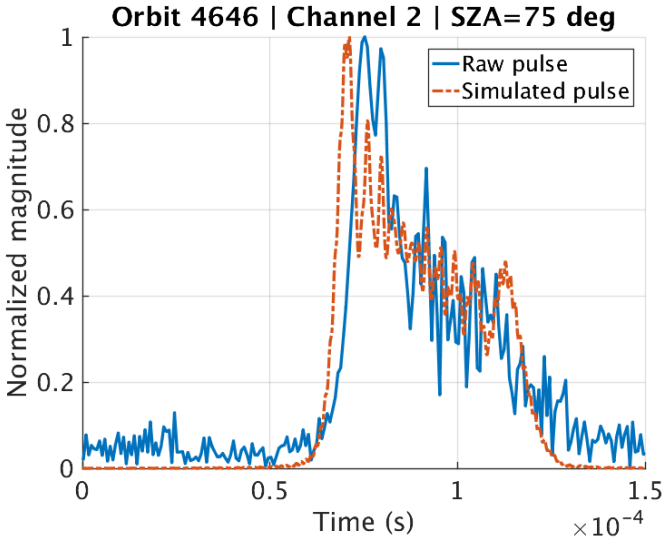

(b) Channel 2.

Figure 2: Blue solid line: raw range-compressed pulses at 75 degrees SZA for orbit 4646. Purple dotted line: Simulated pulses, using parameters obtained from the RMSE routine. All pulses are individually normalized, such that the peak amplitude of each pulse is 1.

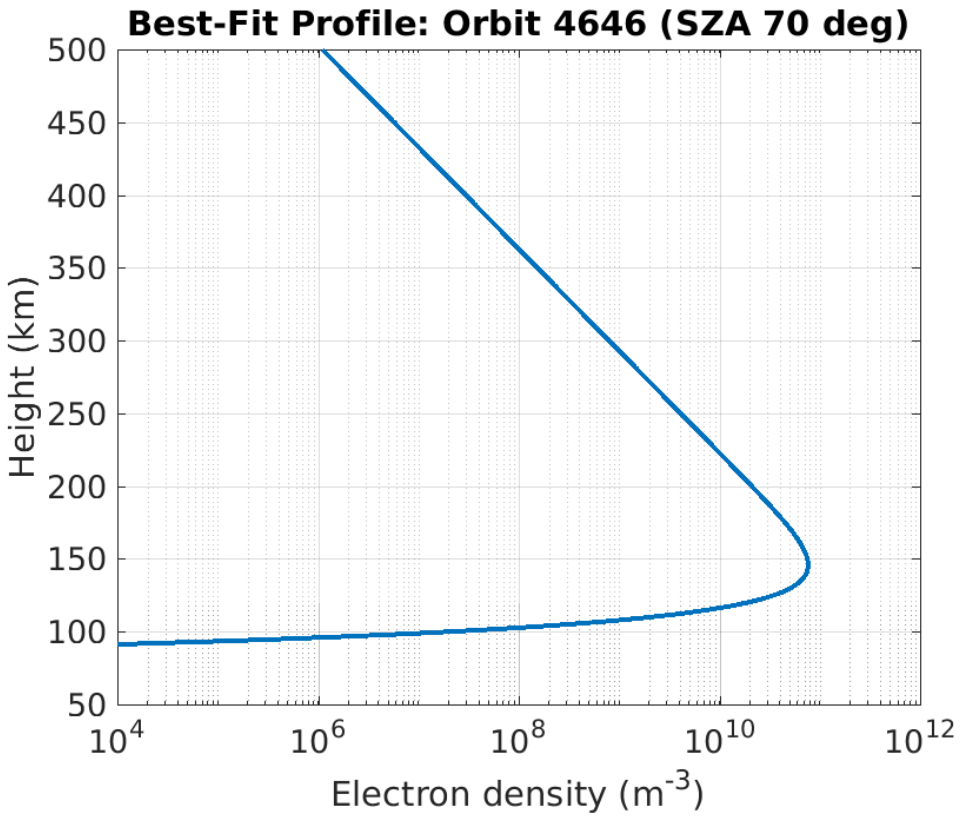

Figure 3: Best-fit electron density profile at SZA 70 degrees for orbit 4646. Note that the shape of the profile scales with SZA as given by equation (15).

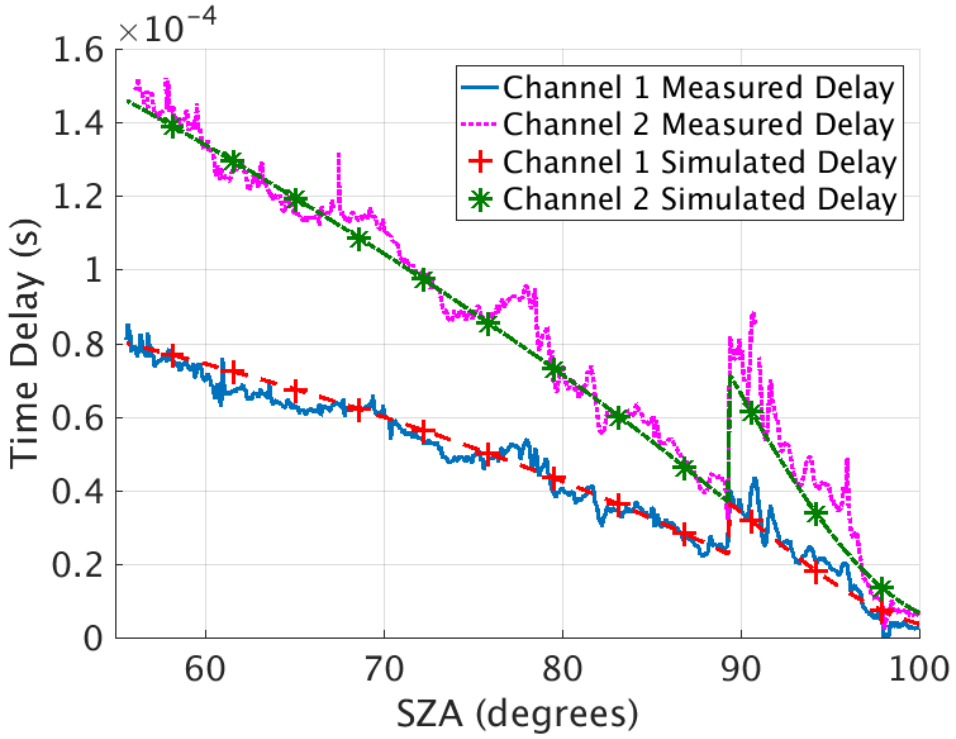

Figure 4: Comparison of measured vs simulated ionospheric delay for orbit 4646. The jump at SZA = 89 degrees is caused by the radar changing to a different set of frequency bands. Channel 1 centre frequency: 4 MHz SZA $>$ 89 degrees, 5 MHz SZA $<$ 89 degrees. Channel 2 centre frequency: 3 MHz SZA $>$ 89 degrees, 4 MHz SZA $<$ 89 degrees. Blue solid line: channel 1 measured delay. Purple dotted line: channel 2 measured delay. Red crosses: channel 1 simulated delay. Green stars: channel 2 simulated delay.

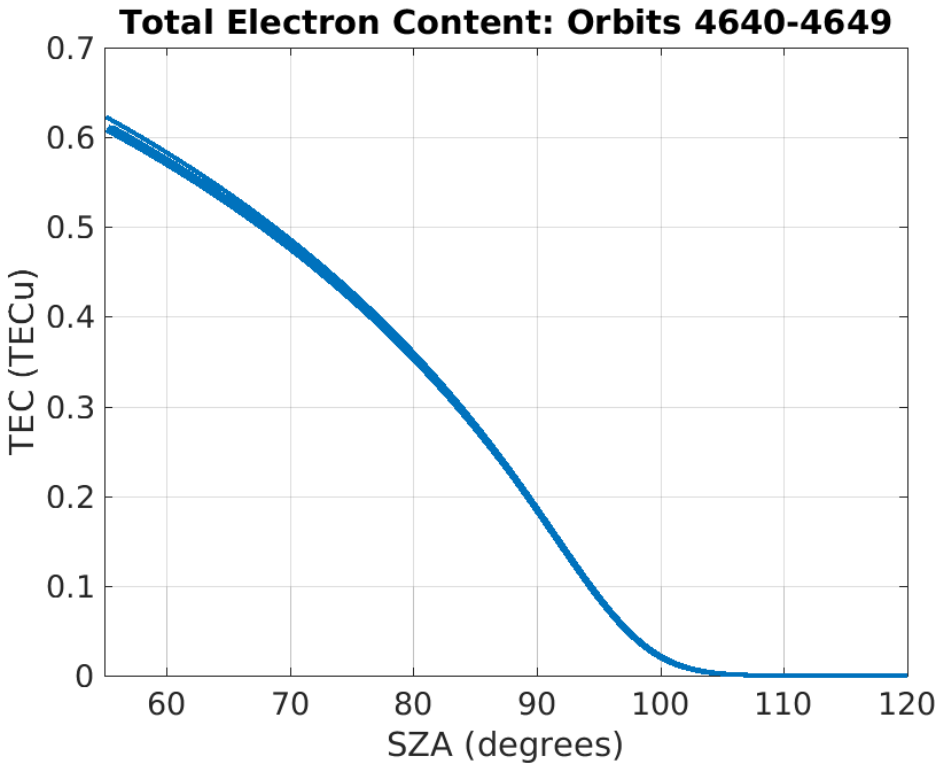

Figure 5: TEC inverted from the best-fit ionospheric profiles for orbits 4640-4649.

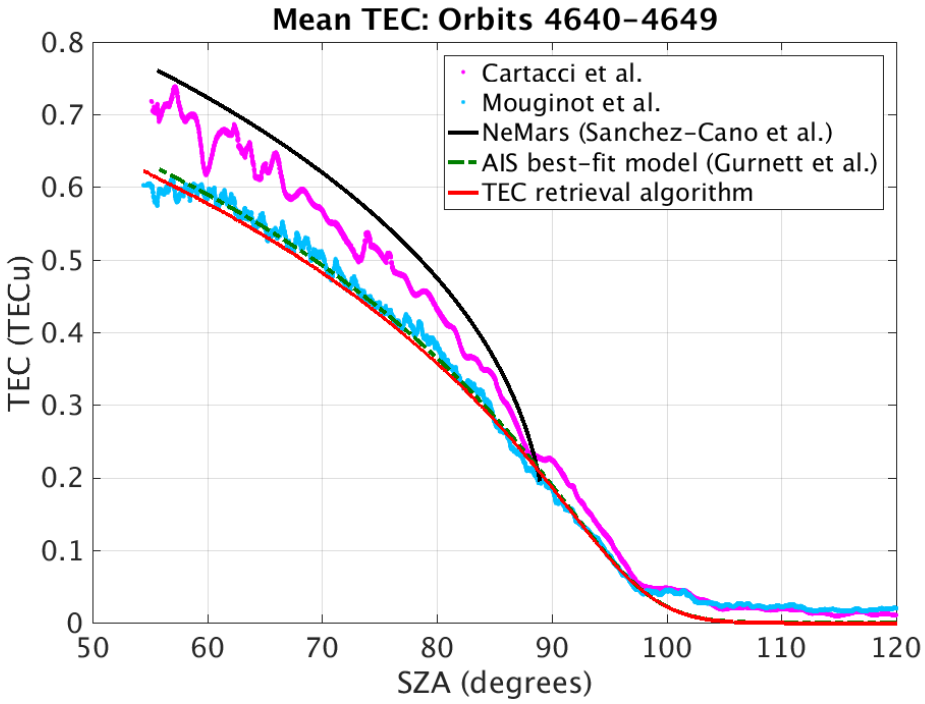

Figure 6: Mean TEC of this study compared to previous studies for orbits 4640-4649. Pink: Cartacci et al. [5]. Light blue: Mouginot et al. [3]. Black: NeMars model [18],[20]. Green: Gurnett et al. best-fit model derived from AIS data [14]. Red: best-fit model found by this study.

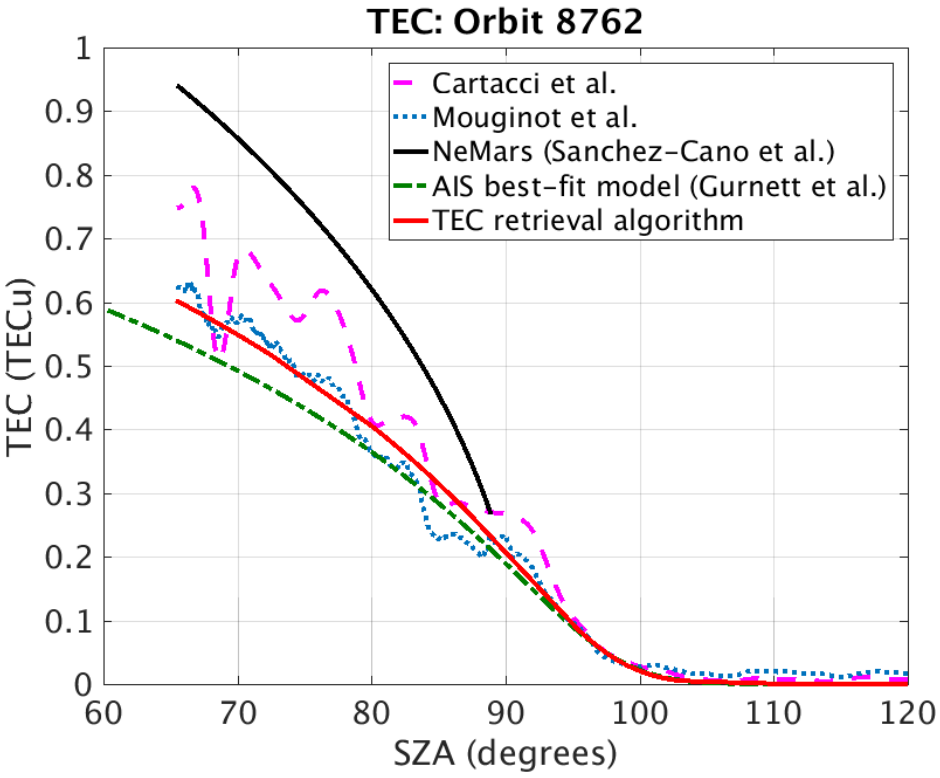

Figure 7: Pink dashed line: Cartacci et al. [5]. Blue dotted line: Mouginot et al. [3]. Black solid line: NeMars model [18],[20]. Green dot-dashed line: Gurnett et al. best-fit model derived from AIS data [14]. Red solid line: best-fit model found by this study.